DOI: 10.13009/EUCASS2019-455

Two-phase gas-particle flow over bodies: modelling and simulation of random effects

Yu.M. Tsirkunov [†], *D.A. Romanyuk and S.V. Panfilov*

[*] *Baltic State Technical University, 1st Krasnoarmeiskaya str. 1, 190005 Saint Petersburg, Russia*
[†] *Corresponding author: tsrknv@bstu.spb.su*

Abstract

An approach to modelling random phenomena, which are typical for actual particle phase in two-phase gas-particle flows, is developed. The collision of non-spherical particles with the wall, scattering of rebounded particles, collisions between particles, and the particle size dispersion are considered. Two kinds of the particle shape are taken in calculations: parallelepiped, and parallelepiped with cut vertices. The three-dimensional particle-wall collision problem is solved numerically using a non-sliding collision model. Scattering indicatrices for non-spherical particles rebounded from a smooth wall surface are studied systematically by direct numerical simulation of rebounding the great number of particles. A kinetic model is used for modelling a "collisional gas" of particles in the carrier gas flow. Particle size distribution is described by the lognormal law. The developed approach is incorporated into the gas-particle flow model, and detailed investigation of the particle phase flow structure is carried out for high-speed gas-particle flow over a blunt body (cylinder). The hierarchy of significance of the considered effects depending on the particles' and flow parameters is constructed. The distribution of the particle energy loss in particle-wall collisions along the body contour is found for particles of different shape. The shielding effect of the particle-particle collisions on the energy loss is discussed.

1. Introduction

The key engineering problems in aerodynamics of high-speed aerospace vehicles intended for flight in the dusty atmosphere can be formulated as follows: (1) how does the dispersed phase influence the drag force and heat transfer, and (2) what are the rate of surface erosion due to particles' impacts. As is seen, the prime and immediate interest is focused on the functionals of a two-phase gas-particle flow. Experimental and theoretical results on the subject obtained by 2007 are accumulated in [1]. Eventually these functionals are determined by the flow structure and the mechanism of particle-wall impact interaction. The investigation of reasons of why a carrier gas and a dispersed phase behave in one way or another leads to the necessity of considering the micro- and macro-phenomena in a two-phase gas-particle medium. The study of these phenomena refers to the fundamentals of the multiphase flow mechanics. From this viewpoint, the key problems include the gas-particle interaction, a collision between two or more particles, the particle-wall interaction, collective effects in a gas-particle mixture and in the flow action on a body surface, the influence of particles on a carrier gas flow parameters and the like. Specific features of particle phase flow patterns over bodies, as well as mathematical models of some "elementary" interactions in such flows and the basic regimes of flows were analyzed in [2]. Different specific aspects of the problem were studied and analyzed later in [3]–[7]. Some of the most important results entered into the review paper [8].

As in known, the classical theory of two-phase gas-particle flow assumes that particles are equal in size, have spherical shape, do not collide with each other, and rebound regularly from streamlined surface. In actual gas-particle flow, these assumptions are not valid. In recent time a considerable number of publications have been devoted to more realistic effects: interaction of non-spherical particles with the carrier gas flow [9]–[12], non-spherical particle-wall collisions [13]–[16], flow of polydisperse particle phase [17].

In spite of considerable efforts of many researchers, many questions remains open. The aim of the present study is to develop theoretical approaches to modelling of some random in nature phenomena in gas-particle flows and to investigate a high-speed dusty gas flow over a blunt body with taking these phenomena into account.

DOI: 10.13009/EUCASS2019-455

2. Three-dimensional particle-wall collision model

A process of non-spherical particle rebound from a solid wall can conclude one or several particle-wall collisions before a particle flies away. At first we consider an isolated collision of a particle with a flat wall and then investigate statistic parameters of rebounded non-spherical particles taking account for all collisions during a rebound. Let $OXYZ$ be the local Cartesian coordinate system with the XZ-plane coincident with the wall surface and the Y-axis normal to it. Denote the coordinates of the particle gravity center by $X_\mathrm{p}, Y_\mathrm{p}, Z_\mathrm{p}$. We introduce also the particle-fixed coordinates $O_\mathrm{p}\xi\eta\zeta$ with the axes directed along the particle principal axes of inertia. The angles φ, ψ, ϑ define the particle orientation with respect to the coordinate system $OXYZ$ (see Fig. 1).

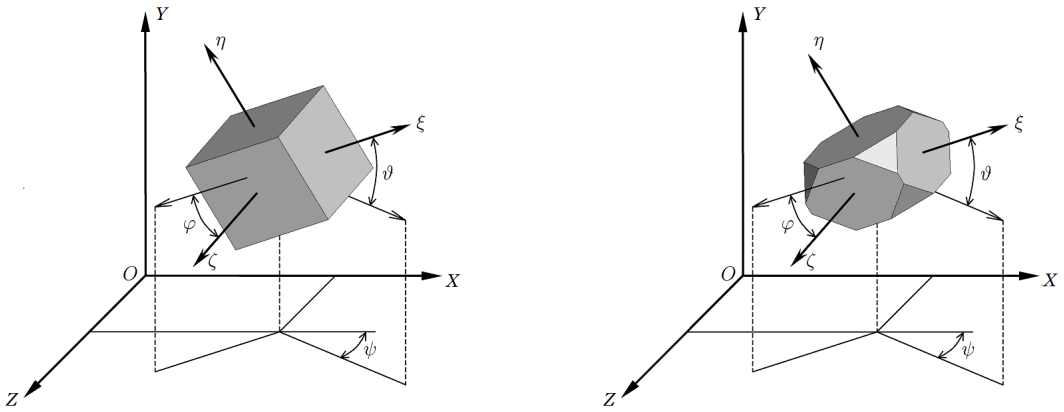

Figure 1: Prismatic particle (rectangular parallelepiped) and prismatic particle with cut vertices; φ, ψ, ϑ are the angles defining particle orientation in space.

The 'hard particle model' [18] will be used in simulating the particle-wall collisions. Let the vectors of the particle translational and angular velocities, $\mathbf{V}_\mathrm{p}$ and $\mathbf{\Omega}_\mathrm{p}$, and the angles φ, ψ, ϑ be known just before a collision. The problem is to determine the post-collisional particle velocities $\mathbf{V}_\mathrm{p}$ and $\mathbf{\Omega}_\mathrm{p}$. Assume that the particle-wall collision occurs at a point which will be designated as the contact point (point C in Fig. 2). If the contact area is an edge or a face of a prismatic particle, we consider the geometric center of the edge or the face as the contact point to avoid an uncertain situation in calculations. The position of the contact point with respect to the particle center of gravity is defined by the vector $\mathbf{r}_c$.

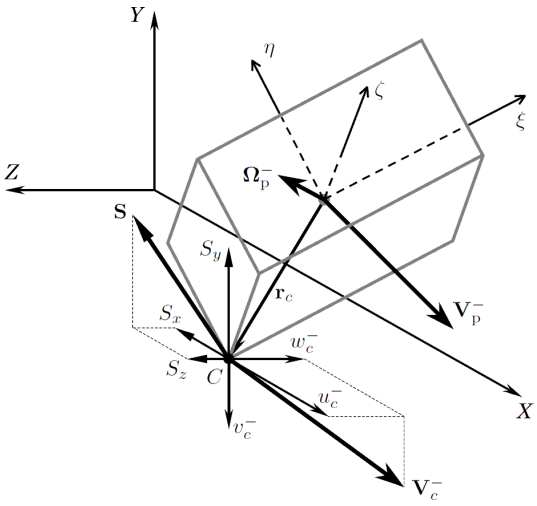

Figure 2: Collision of a non-spherical particle with a wall.

Assuming the collision duration to be very short, so that the particle position relative to the wall surface does not changes during the collision process, write the equations for the change of the particle momentum and angular

DOI: 10.13009/EUCASS2019-455

momentum in the integrated form

$$m_{\rm p}(\mathbf{V}_{\rm p}^{+}-\mathbf{V}_{\rm p}^{-}) \equiv m_{\rm p}\Delta\mathbf{V}_{\rm p} = \int_0^{\delta t} \mathbf{f}_c(t)\mathrm{d}t \equiv \mathbf{S}, \qquad \|J_{\rm p}\|\,(\mathbf{\Omega}_{\rm p}^{+}-\mathbf{\Omega}_{\rm p}^{-}) \equiv \|J_{\rm p}\|\,\Delta\mathbf{\Omega}_{\rm p} = \mathbf{r}_c\times\mathbf{S}, \tag{1}$$

where $m_{\rm p}$, $\|J_{\rm p}\|$ are the mass and inertia tensor of the particle, $\mathbf{f}_c$, $\mathbf{S}$ are the force and the impulse acting on the particle at the contact point, δt is the time interval in which the force $\mathbf{f}_c$ acts on the particle, superscripts "−" and "+" signify the pre- and post-collisional particle parameters (see Fig. 2).

The velocity of the particle contact point $\mathbf{V}_c$, and the particle translational and angular velocities $\mathbf{V}_{\rm p}$ and $\mathbf{\Omega}_{\rm p}$ are related by the kinematic equation

$$\mathbf{V}_c = \mathbf{V}_{\rm p} + \mathbf{\Omega}_{\rm p}\times\mathbf{r}_c. \tag{2}$$

From this we obtain

$$\Delta\mathbf{V}_c \equiv \mathbf{V}_c^{+}-\mathbf{V}_c^{-} = \Delta\mathbf{V}_{\rm p} + \Delta\mathbf{\Omega}_{\rm p}\times\mathbf{r}_c. \tag{3}$$

Combining Eqs. (1) and (3) yields

$$\frac{1}{m_{\rm p}}\|J_{\rm p}\|\,\Delta\mathbf{\Omega}_{\rm p} = \mathbf{r}_c\times\Delta\mathbf{V}_c - \mathbf{r}_c\times[\Delta\mathbf{\Omega}_{\rm p}\times\mathbf{r}_c]. \tag{4}$$

Equation (4) contains two unknown vectors $\Delta\mathbf{V}_c$ and $\Delta\mathbf{\Omega}_{\rm p}$.

Vector $\Delta\mathbf{V}_c$ can be determined if the restitution coefficients of the normal (a_{nc}) and tangential ($a_{\tau c}$) to the surface components of $\mathbf{V}_c$ defined by

$$a_{nc} = -\frac{V_{cn}^{+}}{V_{cn}^{-}}, \quad a_{\tau c} = \frac{V_{c\tau}^{+}}{V_{c\tau}^{-}} \tag{5}$$

are known (here $a_{nc}<0$ because $V_{cn}^{-}<0$ and $V_{cn}^{+}>0$). Actually, a_{nc} and $a_{\tau c}$ depend on the particle and wall material, the particle shape, the collision angle α_1 (see Fig. 3), and the pre-collisional particle parameters. In the present study the coefficient $a_{\tau c}$ is taken to be zero (this corresponds to non-sliding collision) and the coefficient a_{nc} is calulated from the formula

$$a_{nc} = -\exp\left[-0.1(V_{cn}^{-})^{0.61}\right] \tag{6}$$

which is obtained from the empirical correlation suggested in [19], when applied to the pre-collision particle normal velocity. Let $u_{\rm p}$, $v_{\rm p}$, $w_{\rm p}$ and u_c, v_c, w_c be the components of the vectors $\mathbf{V}_{\rm p}$ and $\mathbf{V}_c$ in coordinates $OXYZ$. Then the components Δu_c, Δv_c and Δw_c of the vector $\Delta\mathbf{V}_c$ can be expressed through the components of the vector $\mathbf{V}_c^{-}$ and the coefficients a_{nc} and $a_{\tau c}$ as follows:

$$\Delta u_c = -u_c^{-}, \qquad \Delta v_c = -(a_{nc}+1)v_c^{-}, \qquad \Delta w_c = -w_c^{-}. \tag{7}$$

It is convenient to describe the particle rotational movement using the particle-fixed coordinates $O_{\rm p}\xi\eta\zeta$ because the tensor $\|J_{\rm p}\|$ has in this case only diagonal non-zero components $J_{{\rm p}\xi}$, $J_{{\rm p}\eta}$, $J_{{\rm p}\zeta}$, which are the principal moments of inertia of the particle. The vector equation (4) written in the coordinates $O_{\rm p}\xi\eta\zeta$ has the form

$$\begin{aligned}
\hat{J}_{{\rm p}\xi}\Delta\omega_{{\rm p}\xi} &= (\eta_c\Delta V_{c\zeta}-\zeta_c\Delta V_{c\eta}) - \eta_c^2\Delta\omega_{{\rm p}\xi} + \xi_c\eta_c\Delta\omega_{{\rm p}\eta} + \xi_c\zeta_c\Delta\omega_{{\rm p}\zeta} - \zeta_c^2\Delta\omega_{{\rm p}\xi},\\
\hat{J}_{{\rm p}\eta}\Delta\omega_{{\rm p}\eta} &= (\zeta_c\Delta V_{c\xi}-\xi_c\Delta V_{c\zeta}) - \zeta_c^2\Delta\omega_{{\rm p}\eta} + \eta_c\zeta_c\Delta\omega_{{\rm p}\zeta} + \eta_c\xi_c\Delta\omega_{{\rm p}\xi} - \xi_c^2\Delta\omega_{{\rm p}\eta},\\
\hat{J}_{{\rm p}\zeta}\Delta\omega_{{\rm p}\zeta} &= (\xi_c\Delta V_{c\eta}-\eta_c\Delta V_{c\xi}) - \xi_c^2\Delta\omega_{{\rm p}\zeta} + \zeta_c\xi_c\Delta\omega_{{\rm p}\xi} + \zeta_c\eta_c\Delta\omega_{{\rm p}\eta} - \eta_c^2\Delta\omega_{{\rm p}\zeta}.
\end{aligned} \tag{8}$$

Here $\hat{J}_{{\rm p}i} = J_{{\rm p}i}/m_{\rm p}$ ($i=\xi,\,\eta,\,\zeta$), and ξ_c, η_c, ζ_c are the components of the position vector $\mathbf{r}_c$. The relations (8) represent the system of the linear algebraic equations for the unknown values $\Delta\omega_{{\rm p}\xi}$, $\Delta\omega_{{\rm p}\eta}$ and $\Delta\omega_{{\rm p}\zeta}$. It can be rewritten in the matrix form as

$$\begin{pmatrix} \hat{J}_{{\rm p}\xi}+\eta_c^2+\zeta_c^2 & -\xi_c\eta_c & -\xi_c\zeta_c \\ -\eta_c\xi_c & \hat{J}_{{\rm p}\eta}+\zeta_c^2+\xi_c^2 & -\eta_c\zeta_c \\ -\zeta_c\xi_c & -\zeta_c\eta_c & \hat{J}_{{\rm p}\zeta}+\xi_c^2+\eta_c^2 \end{pmatrix} \begin{pmatrix} \Delta\omega_{{\rm p}\xi} \\ \Delta\omega_{{\rm p}\eta} \\ \Delta\omega_{{\rm p}\zeta} \end{pmatrix} = \begin{pmatrix} \eta_c\Delta V_{c\zeta}-\zeta_c\Delta V_{c\eta} \\ \zeta_c\Delta V_{c\xi}-\xi_c\Delta V_{c\zeta} \\ \xi_c\Delta V_{c\eta}-\eta_c\Delta V_{c\xi} \end{pmatrix}, \tag{9}$$

Once a solution of (9) is found, the components of $\mathbf{\Omega}_{\rm p}^{+}$ in the particle-fixed coordinates can be easily obtained:

$$\omega_{{\rm p}\xi}^{+} = \omega_{{\rm p}\xi}^{-} + \Delta\omega_{{\rm p}\xi}, \qquad \omega_{{\rm p}\eta}^{+} = \omega_{{\rm p}\eta}^{-} + \Delta\omega_{{\rm p}\eta}, \qquad \omega_{{\rm p}\zeta}^{+} = \omega_{{\rm p}\zeta}^{-} + \Delta\omega_{{\rm p}\zeta}. \tag{10}$$

Determine a velocity vector $\mathbf{V}_{\rm p}^{+}$ in the coordinates $OXYZ$ connected with the wall surface. The direction of $\mathbf{V}_{\rm p}^{+}$ coincides with the direction of movement of a particle just after its collision. The vector $\mathbf{V}_{\rm p}^{+}$ can be expressed from (3) as follows

$$\mathbf{V}_{\rm p}^{+} = \mathbf{V}_{\rm p}^{-} + \Delta\mathbf{V}_{\rm p} = \mathbf{V}_{\rm p}^{-} + \Delta\mathbf{V}_c - \Delta\mathbf{\Omega}_{\rm p}\times\mathbf{r}_c. \tag{11}$$

DOI: 10.13009/EUCASS2019-455

In a two-phase gas-particle flow, the velocity vector of a particle just before its collision $\mathbf{V}_\mathrm{p}^-$ can be determined from the particle trajectory computation. Hence, we consider the components u_p^-, v_p^-, w_p^- in $OXYZ$-coordinates as the known values. The components of the vector ${}_\Delta\mathbf{V}_c$ in these coordinates are given by the relations (7) in which u_c^-, v_c^-, w_c^- can be found from the kinematic relation (2). Thus, the problem is to determine the components of vectors ${}_\Delta\mathbf{\Omega}_\mathrm{p}$ and $\mathbf{r}_c$ in $OXYZ$-coordinates, whereas we know their components in the particle-fixed coordinates $O_\mathrm{p}\xi\eta\zeta$. The components of any vector $\mathbf{b}$ in the coordinate systems $OXYZ$ and $O_\mathrm{p}\xi\eta\zeta$ are related by

$$\begin{pmatrix} b_\xi \\ b_\eta \\ b_\zeta \end{pmatrix} = \mathbf{A}\begin{pmatrix} b_X \\ b_Y \\ b_Z \end{pmatrix}, \qquad \begin{pmatrix} b_X \\ b_Y \\ b_Z \end{pmatrix} = \mathbf{A}^\mathrm{T}\begin{pmatrix} b_\xi \\ b_\eta \\ b_\zeta \end{pmatrix}, \tag{12}$$

where $\mathbf{A}$ is the rotation matrix the elements of which can be expressed through the angles φ, ψ, ϑ, and $\mathbf{A}^\mathrm{T}$ is the transposed matrix ($\mathbf{A}^\mathrm{T}$ coincides with the inverse matrix $\mathbf{A}^{-1}$). However, it is much more convenient to describe the particle rotation in terms of the Rodrigues-Hamilton parameters rather then in terms of the Eulerian angles, because in this case the system of the kinematic equations has no singularities. Formally, it means that we go from φ, ψ, ϑ to new variables λ_k (k = 0, 1, 2, 3), which are related with φ, ψ, ϑ by

$$\begin{aligned}
\lambda_0 &= \cos(\varphi/2)\cos(\psi/2)\cos(\vartheta/2) - \sin(\varphi/2)\sin(\psi/2)\sin(\vartheta/2),\\
\lambda_1 &= \sin(\varphi/2)\cos(\psi/2)\cos(\vartheta/2) + \cos(\varphi/2)\sin(\psi/2)\sin(\vartheta/2),\\
\lambda_2 &= \cos(\varphi/2)\sin(\psi/2)\cos(\vartheta/2) + \sin(\varphi/2)\cos(\psi/2)\sin(\vartheta/2),\\
\lambda_3 &= \cos(\varphi/2)\cos(\psi/2)\sin(\vartheta/2) - \sin(\varphi/2)\sin(\psi/2)\cos(\vartheta/2).
\end{aligned} \tag{13}$$

The elements of matrix $\mathbf{A}$ are expressed in terms of λ_k as

$$\begin{aligned}
a_{11} &= \lambda_0^2 + \lambda_1^2 - \lambda_2^2 - \lambda_3^2, & a_{12} &= 2(\lambda_0\lambda_3 + \lambda_1\lambda_2), & a_{13} &= 2(\lambda_1\lambda_3 - \lambda_0\lambda_2),\\
a_{21} &= 2(\lambda_1\lambda_2 - \lambda_0\lambda_3), & a_{22} &= \lambda_0^2 - \lambda_1^2 + \lambda_2^2 - \lambda_3^2, & a_{23} &= 2(\lambda_0\lambda_1 + \lambda_2\lambda_3),\\
a_{31} &= 2(\lambda_0\lambda_2 + \lambda_3\lambda_1), & a_{32} &= 2(\lambda_2\lambda_3 - \lambda_0\lambda_1), & a_{33} &= \lambda_0^2 - \lambda_1^2 - \lambda_2^2 + \lambda_3^2.
\end{aligned} \tag{14}$$

If the angles φ, ψ, ϑ are given, we can calculate the values of λ_0, λ_1, λ_2, λ_3 from (13), and then the elements of the matrix $\mathbf{A}$ from (14). With this result we obtain from (12)

$$\begin{pmatrix} \omega_{\mathrm{p}X} \\ \omega_{\mathrm{p}Y} \\ \omega_{\mathrm{p}Z} \end{pmatrix} = \mathbf{A}^\mathrm{T}\begin{pmatrix} \omega_{\mathrm{p}\xi} \\ \omega_{\mathrm{p}\eta} \\ \omega_{\mathrm{p}\zeta} \end{pmatrix}, \qquad \begin{pmatrix} \Delta\omega_{\mathrm{p}X} \\ \Delta\omega_{\mathrm{p}Y} \\ \Delta\omega_{\mathrm{p}Z} \end{pmatrix} = \mathbf{A}^\mathrm{T}\begin{pmatrix} \Delta\omega_{\mathrm{p}\xi} \\ \Delta\omega_{\mathrm{p}\eta} \\ \Delta\omega_{\mathrm{p}\zeta} \end{pmatrix}, \qquad \begin{pmatrix} r_{cX} \\ r_{cY} \\ r_{cZ} \end{pmatrix} = \mathbf{A}^\mathrm{T}\begin{pmatrix} \xi_c \\ \eta_c \\ \zeta_c \end{pmatrix}. \tag{15}$$

Substitution of $\omega_{\mathrm{p}\xi}, \omega_{\mathrm{p}\eta}, \omega_{\mathrm{p}\zeta}$ from (10) into the first relation in (15) gives the components of $\mathbf{\Omega}_\mathrm{p}^+$ in the $OXYZ$-coordinates. Substituting the values of $\Delta\omega_{\mathrm{p}X}, \Delta\omega_{\mathrm{p}Y}, \Delta\omega_{\mathrm{p}Z}$ and r_{cX}, r_{cY}, r_{cZ} from (15) to (11) we obtain the final expressions for the components of the vector $\mathbf{V}_\mathrm{p}^+$ in the system of coordinates $OXYZ$

$$\begin{aligned}
u_\mathrm{p}^+ &= u_\mathrm{p}^- + \Delta u_c - \Delta\omega_{\mathrm{p}Y} r_{cZ} + \Delta\omega_{\mathrm{p}Z} r_{cY},\\
v_\mathrm{p}^+ &= v_\mathrm{p}^- + \Delta v_c - \Delta\omega_{\mathrm{p}Z} r_{cX} + \Delta\omega_{\mathrm{p}X} r_{cZ},\\
w_\mathrm{p}^+ &= w_\mathrm{p}^- + \Delta w_c - \Delta\omega_{\mathrm{p}X} r_{cY} + \Delta\omega_{\mathrm{p}Y} r_{cX}.
\end{aligned} \tag{16}$$

Thus, if we have the velocity of the particle center of gravity $\mathbf{V}_\mathrm{p}^-$, the particle angular velocity $\mathbf{\Omega}_\mathrm{p}^-$, and the angles φ, ψ, ϑ at the moment of a particle-wall collision, we can calculate the components of the velocity of the particle center of gravity and the particle angular velocity just after a collision in XYZ-coordinates using the relations (2), (7), (9), (10), (13), (14), (15), and (16). Note, that the position vector $\mathbf{r}_c$ is defined uniquely by the particle shape and the particle orientation at the moment of a collision.

3. Scattering of rebounded particles

Non-spherical particles impinging on a wall at a given angle on incidence α_1 (see Fig. 3) and with the same translational and rotational velocities, $\mathbf{V}_{\mathrm{p}1}$ and $\mathbf{\Omega}_{\mathrm{p}1}$, rebound in different directions. Such a phenomenon is referred to as the particle scattering. It is caused by the random orientation of particles in space before the first collision. A particle can experience several collisions during one rebound. We use the particle-wall collision model described in the previous Section for each collision.

DOI: 10.13009/EUCASS2019-455

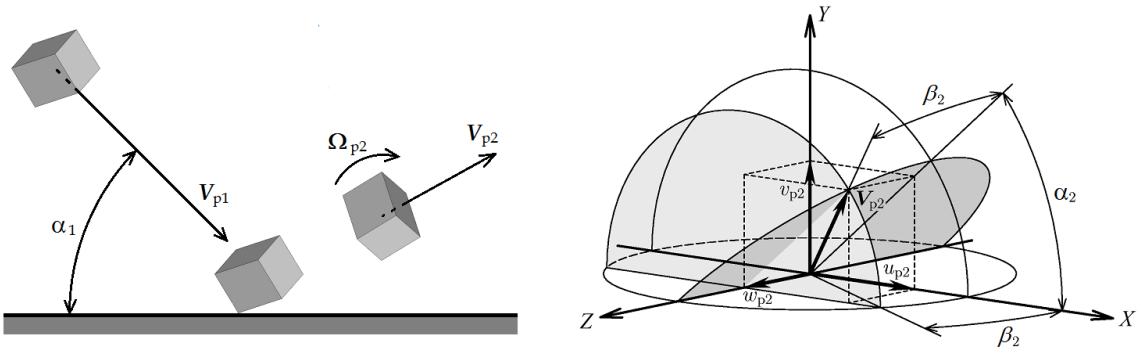

Figure 3: Schematic of a particle impact: angles α_2 and β_2 define the direction of a particle rebound.

Let (XY) be the plane of impact (the plane in which vector $\mathbf{V}_{p1}$ and the normal to the wall surface lie). The direction of the particle rebound can be defined by two angles α_2 and β_2 (Fig. 3). The angle α_2 lies in the range from 0 to π, and the angle β_2 from $-\pi/2$ to $\pi/2$.

Let N be a number of incident particles with the fixed $\mathbf{V}_{p1}$, $\mathbf{\Omega}_{p1}$ and α_1, and $dN(\alpha_2,\beta_2,d\alpha_2,d\beta_2)$ be a number of those particles, which are reflected in the direction specified by the intervals of angles $[\alpha_2,\alpha_2+d\alpha_2]$ and $[\beta_2,\beta_2+d\beta_2]$. Introduce the distribution function $I(\alpha_2,\beta_2)$ of rebounded particles over the angles α_2 and β_2 by the relationship $I(\alpha_2,\beta_2)\,d\alpha_2\,d\beta_2 = dN(\alpha_2,\beta_2,d\alpha_2,d\beta_2)/N$. This expression represents the probability of particle rebound in the direction defined by the angles (α_2,β_2) within the intervals $d\alpha_2$ and $d\beta_2$, respectively. The function $I(\alpha_2,\beta_2)$ will be referred to as the three-dimensional (3D) scattering indicatrix. Integrating $I(\alpha_2,\beta_2)$ over β_2 from $-\pi/2$ to $\pi/2$ we obtain the two-dimensional (2D) scattering indicatrix which describes the distribution of rebounded particles over the angle α_2 (denote it by $F(\alpha_2)$).

The scattering indicatrices for particles rebounded from a smooth solid wall were calculated using the direct statistical simulation technique. In the domain of angles $0 \leqslant \alpha_2 \leqslant \pi$ and $-\pi/2 \leqslant \beta_2 \leqslant \pi/2$, we introduced the uniform rectangular grid with the steps $\Delta\alpha_2 = \Delta\beta_2 = \pi/180$ $(= 1^\circ)$. The rebound of a great number of particles $(\approx 5\cdot 10^7)$ was simulated for initially non-rotating particles ($\mathbf{\Omega}_{p1} = 0$) at fixed ($\mathbf{V}_{p1}$ and α_1).

In calculations, the particle shape parameters were taken as follows: for prisms (the extended parallelepiped) the aspect ratios were taken as $b/a = c/a = 0.8$, and for prisms with cut vertices the aspect ratios were taken as $b/a = 0.6$, $c/a = 0.8$. The size a had no effect on the indicatrices. Initial space orientation of a particle in every trial was considered as random and equiprobable. The collision model described above (with restitution coefficients $a_{\tau c} = 0$ and a_{nc} calculated from relationship (6)) was used for every collision of a test particle during its rebound. For (ij)-cell of the grid, the value N_{ij} was determined as a number of particles with rebound angles α_2 and β_2 lying in the intervals $(i-1)\Delta\alpha_2 \leqslant \alpha_2 < i\Delta\alpha_2$, $(j-1)\Delta\beta_2 \leqslant \beta_2 < j\Delta\beta_2$. For large enough N, the ratio N_{ij}/N is close to the probability of reflection of a particle in the direction defined by the above indicated intervals of the angles. Then an approximate value of the function I in the cell (ij) is calculated as

$$I(\alpha_2,\beta_2)_{ij} \approx \frac{N_{ij}}{N\,\Delta\alpha_2\,\Delta\beta_2\,\cos[\Delta\alpha_2(i+1/2)]}.$$

As the values of $I(\alpha_2,\beta_2)_{ij}$ were calculated in all grid cells, the distribution function $I(\alpha_2,\beta_2)$ in the whole calculation domain was constructed. Views of 3D scattering indicatrices for normal impact $(\alpha_1 = 90^\circ)$ of particles of two different shape is shown in Fig. 4.

Distribution of incident particles in a number of particle-wall collisions during a single rebound of every test particle is illustrated by Table 1. The particle impact velocity and the angle of incidence are the same as in Fig. 4. It is clearly seen, that the great majority of test particles experienced more than one collision.

Two-dimensional (2D) scattering indicatrices $F(\alpha_2)$ in the plane XY) was constructed from the calculated values

$$F(\alpha_2)_i \approx \frac{\sum\limits_j N_{ij}}{N\,\Delta\alpha_2},$$

where the summation was over all cells (ij) with the fixed index i. These indicatrices are shown in Fig. 5. The dominant direction of rebound of both considered particle shape differs substantially from that of spherical particles (shown by dotted red lines).

DOI: 10.13009/EUCASS2019-455

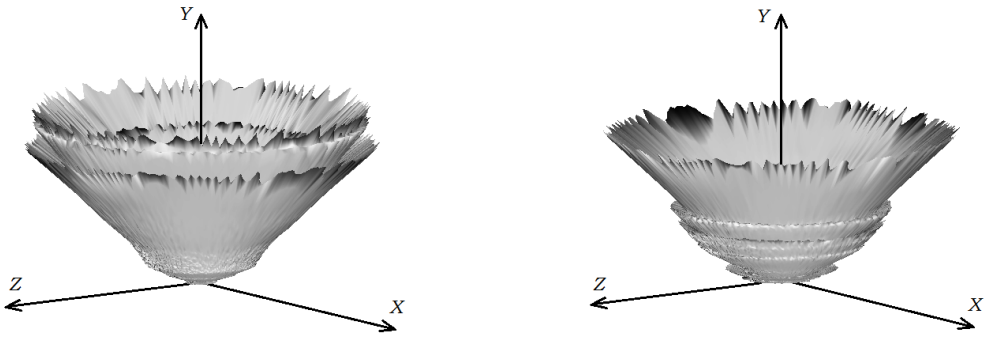

Figure 4: 3D scattering indicatrices of rebounded particles: prismatic particles (left) and prismatic particles with cut vertices (right). V_{p1} = 500 m/s, the incident angle $\alpha_1 = 90°$.

Table 1: Distribution of incident particles in a number of particle-wall collisions during rebound

Number of collisions of an incident particle with the wall during its rebound, K		1	2	3	4	5 and more
Mean part of particles experienced K collisions during a rebound (in percent of a total number of incident particles)	Prismatic particles	2.9	54.1	37.7	5.2	0.1
	Prismatic particles with cut vertices	5.4	39.2	28.2	17.5	9.7

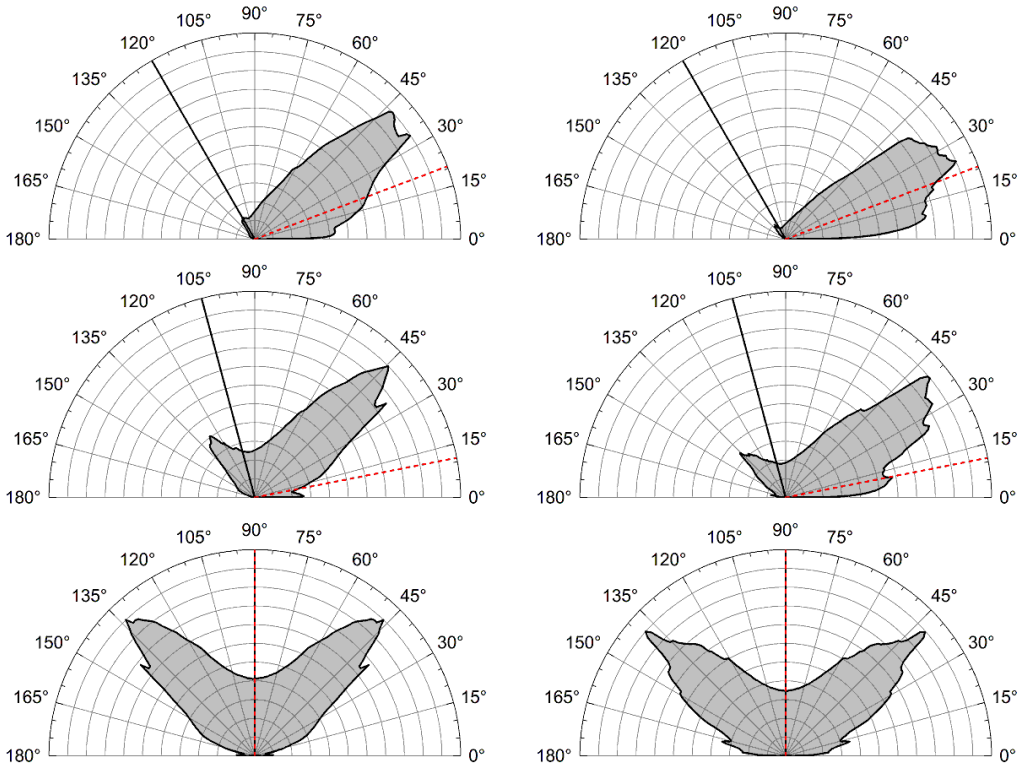

Figure 5: 2D scattering indicatrices of rebounded prismatic particles (left column) and prismatic particles with cut vertices (right column) in the plane of impact (XY). Direction of incident particles' motion is shown by solid black line; direction of spherical particles' rebound is shown by red dotted lines.

DOI: 10.13009/EUCASS2019-455

4. Model of particle-phase motion with particle-particle collisions in gas-particle flow

Particles are more inertial than the carrier gas, and they do not follow the streamlines. Motion of particles in the flow over a body is governed by the gas-particle interaction, inter-particle collisions and impactive interaction of particles with the body surface. Solid particles colliding the body surface rebound from it and then they can collide with the incident ones. These collisions, being random in nature, result in chaotic motion of particles. In this Section we describe briefly a kinetic model for the collisional "gas" of dispersed particles proposed in [20].

Particles are assumed to be spheres of the same radius r_p. They interact with each other only through binary collisions that is valid if the "gas" of particles is not too dense. Besides, it is assumed that collision process is instantaneous and the position of colliding particles does not change during a collision. The state of the i-th particle is determined by a point $\mathbf{x}_i$ of the phase space which includes the particle position vector $\mathbf{r}_i$, the particle translational and rotational velocities ($\mathbf{v}_{\mathrm{p}i}$ and $\mathbf{\Omega}_{\mathrm{p}i}$, respectively), i.e. $\mathbf{x}_i = (\mathbf{r}_i, \mathbf{v}_{\mathrm{p}i}, \mathbf{\Omega}_{\mathrm{p}i})$. The vector $\mathbf{x}_i$ is split into $\mathbf{r}_i$ and $\mathbf{y}_i = (\mathbf{v}_{\mathrm{p}i}, \mathbf{\Omega}_{\mathrm{p}i})$. We denote the parameters of the i-th and j-th particles before and after their collision by the superscripts "$-$" and "$+$", respectively. The post-collisional parameters of colliding particles are fully determined by the pre-collisional ones and the relative position of particles at the collision instant, thus we can write $\mathbf{y}_k^+ = \mathbf{y}_k^+(\mathbf{y}_i^-, \mathbf{y}_j^-, \mathbf{n}_{ij})$, $k = i, j$, where $\mathbf{n}_{ij}$ is the unit vector directed from the centre of i-th particle towards the centre of j-th particle at the instant of collision. The above relation for $\mathbf{y}_k^+$ is presumed to give a one-to-one correspondence between $\mathbf{y}_k^-$ and $\mathbf{y}_k^+$, so that the Jacobian $J_1 = |D(\mathbf{y}_i^+, \mathbf{y}_j^+)/D(\mathbf{y}_i^-, \mathbf{y}_j^-)| \neq 0$ and, hence, the relation can be resolved for the particle parameters before a collision $\mathbf{y}_k^- = \mathbf{y}_k^-(\mathbf{y}_i^+, \mathbf{y}_j^+, \mathbf{n}_{ij})$, $k = i, j$. A collision is physically feasible only when $\mathbf{g}_{ij}^- \cdot \mathbf{n}_{ij} \leq 0$, where $\mathbf{g}_{ij} = \mathbf{v}_j - \mathbf{v}_i$. We assume also that states of any two particles in the phase space are not statistically correlated. This assumption is valid if the mean free path of particles moving in the carrier gas is much smaller than the particle momentum response length. These assumptions and reasoning are similar to those accepted in rarefied gas dynamics for collisions between molecules.

Let $f_1 = f(\mathbf{x}_1, t)$ be the distribution function such that $f_1\, d\mathbf{x}_1 = f(\mathbf{r}_1, \mathbf{v}_{\mathrm{p}1}, \mathbf{\Omega}_{\mathrm{p}1}, t)\, d\mathbf{r}_1\, d\mathbf{v}_{\mathrm{p}1}\, d\mathbf{\Omega}_{\mathrm{p}1}$ is the number of particles with coordinates and velocities from the elementary volume $d\mathbf{r}_1\, d\mathbf{v}_{\mathrm{p}1}\, d\mathbf{\Omega}_{\mathrm{p}1}$ in the vicinity of the point $\mathbf{x}_1 = (\mathbf{r}_1, \mathbf{v}_{\mathrm{p}1}, \mathbf{\Omega}_{\mathrm{p}1})$ of the phase space. Then, the following kinetic Boltzmann-type equation for f_1 can be derived

$$\frac{\partial f_1}{\partial t} + \frac{\partial}{\partial \mathbf{r}_1}(\mathbf{v}_{\mathrm{p}1} f_1) + \frac{\partial}{\partial \mathbf{v}_{\mathrm{p}1}}\left(\frac{\mathbf{f}_{\mathrm{p}1}}{m_\mathrm{p}} f_1\right) + \frac{\partial}{\partial \mathbf{\Omega}_{\mathrm{p}1}}\left(\frac{\mathbf{l}_{\mathrm{p}1}}{I_\mathrm{p}} f_1\right) = I_\mathrm{coll}\,. \tag{17}$$

This equation is a particular case of the more general kinetic equation [20] which also takes gas-particle heat transfer and particle size distribution into account. The collisional integral in the right-hand side is given by

$$I_\mathrm{coll} = 4 r_\mathrm{p}^2 \int d\mathbf{y}_2 \int\limits_{\mathbf{g}_{12}\cdot\mathbf{n}_{12}\leq 0} \left(\frac{f_1^- f_2^-}{J} - f_1 f_2\right) |\mathbf{g}_{12}\cdot\mathbf{n}_{12}| \sin\chi_{12} d\chi_{12} d\varepsilon_{12}, \qquad J = \left|\frac{\mathbf{g}_{12}\cdot\mathbf{n}_{12}}{\mathbf{g}_{12}^-\cdot\mathbf{n}_{12}} J_1\right|. \tag{18}$$

Here m_p and I_p are the particle mass and moment of inertia, $\mathbf{f}_{\mathrm{p}1}$ and $\mathbf{l}_{\mathrm{p}1}$ are the force and the torque acting on a particle from the carrier gas which are calculated for the particle with the parameters $(\mathbf{v}_{\mathrm{p}1}, \mathbf{\Omega}_{\mathrm{p}1})$ at the point $\mathbf{r}_1$ of flow, $f_2 = f(\mathbf{r}_1, \mathbf{y}_2, t)$, $f_1^- = f(\mathbf{r}_1, \mathbf{y}_1^-, t)$, $f_2^- = f(\mathbf{r}_1, \mathbf{y}_2^-, t)$, $\mathbf{g}_{12} = \mathbf{v}_{\mathrm{p}2} - \mathbf{v}_{\mathrm{p}1}$ and $\mathbf{n}_{12}$ has been defined above. The inequality $\mathbf{g}_{12}\cdot\mathbf{n}_{12} \leq 0$ is the condition of physical feasibility of a collision between the 1-st and the 2-nd particles, and the angles χ_{12} and ε_{12} specify the direction of $\mathbf{n}_{12}$ in spherical coordinates with the origin at the centre of the 1-st particle [20].

The function J which enters into the collisional integral depends on the particle-particle collision model which will be discussed later.

Let $\Phi = \Phi(\mathbf{x}_i)$ be a parameter of an individual particle. If a hydrodynamic parameter of a "gas" of particles (in other words, macroparameter of the dispersed phase) $\langle\Phi\rangle(\mathbf{r}, t)$ at a point $\mathbf{r}$ of the physical space is defined as the ensemble averaged value of $\Phi = \Phi(\mathbf{x}_i)$ in a unit volume of the gas–particle mixture, then $\langle\Phi\rangle(\mathbf{r}, t)$ can be expressed in terms of Φ and $f(\mathbf{x}_1, t)$ as follows:

$$\langle\Phi\rangle(\mathbf{r}, t) = \int \Phi(\mathbf{r}, \mathbf{y}_1, t) f(\mathbf{r}, \mathbf{y}_1, t)\, d\mathbf{y}_1. \tag{19}$$

For example, the particle numerical density n_p, the particle volume fraction α_p, the hydrodynamic velocity $\mathbf{w}_\mathrm{p}$ and the specific energy of the particle chaotic motion e_p are calculated as follows:

$$n_\mathrm{p} = \langle 1\rangle, \quad \alpha_\mathrm{p} = \frac{4}{3}\pi r_\mathrm{p}^3 n_\mathrm{p}, \quad \mathbf{w}_\mathrm{p} = \frac{\langle \mathbf{v}_\mathrm{p}\rangle}{n_\mathrm{p}}, \quad e_\mathrm{p} = \frac{1}{m_\mathrm{p} n_\mathrm{p}}\left\langle \frac{m_\mathrm{p}(\mathbf{v}_\mathrm{p} - \mathbf{w}_\mathrm{p})^2}{2}\right\rangle.$$

A model of an non-completely elastic collision between two particles is an important part of the kinetic model. The momentum and angular momentum balance equations for a pair of i-th and j-th colliding spherical particles can

DOI: 10.13009/EUCASS2019-455

be written in the form:

$$m_{\rm p}\mathbf{v}^-_{{\rm p}i} + m_{\rm p}\mathbf{v}^-_{{\rm p}j} = m_{\rm p}\mathbf{v}^+_{{\rm p}i} + m_{\rm p}\mathbf{v}^+_{{\rm p}j}, \qquad I_{\rm p}(\mathbf{\Omega}^+_{{\rm p}k} - \mathbf{\Omega}^-_{{\rm p}k}) = m_{\rm p} r_{\rm p}\mathbf{e}_k \times (\mathbf{v}^+_{{\rm p}k} - \mathbf{v}^-_{{\rm p}k}), \qquad k = i, j, \tag{20}$$

where $\mathbf{e}_i = \mathbf{n}_{ij}$, $\mathbf{e}_j = -\mathbf{n}_{ij}$. The system of these three equations is not closed because it involves four unknowns $\mathbf{v}^+_{{\rm p}k}$ and $\mathbf{\Omega}^+_{{\rm p}k}$, $k = i, j$. Some additional hypotheses for the interaction between particles should be introduced to make this system closed. Considering the relative velocity of particles at the contact point

$$\mathbf{U}_{ij} = \mathbf{v}_{{\rm p}j} - \mathbf{v}_{{\rm p}i} - r_{\rm p}(\mathbf{\Omega}_{{\rm p}i} + \mathbf{\Omega}_{{\rm p}j}) \times \mathbf{n}_{ij} \tag{21}$$

we represent $\mathbf{U}^+_{ij}$ in the form

$$\mathbf{U}^+_{ij} = -a_{{\rm p}n}\mathbf{U}^-_{ij(n)} + a_{{\rm p}t}\mathbf{U}^-_{ij(t)}, \tag{22}$$

where $a_{{\rm p}n}$ and $a_{{\rm p}t}$ are the restitution coefficients of the normal ($\mathbf{U}_{ij(n)} = (\mathbf{U}_{ij}\cdot\mathbf{n}_{ij})\mathbf{n}_{ij}$) and tangential ($\mathbf{U}_{ij(t)} = \mathbf{U}_{ij} - \mathbf{U}_{ij(n)}$) components of the relative velocity $\mathbf{U}_{ij}$. These coefficients are assumed to take into account the losses of the particles' kinetic energy due to inelastic collisions ($a_{{\rm p}n}$) and due to the particles' surface friction ($a_{{\rm p}t}$). Their values lie in the ranges: $0 \le a_{{\rm p}n} \le 1$, $-1 \le a_{{\rm p}t} \le 1$.

The true values of $a_{{\rm p}n}$ and $a_{{\rm p}t}$ in different conditions of a collision are unknown. We assume these restitution coefficients to be constant. If the values of $a_{{\rm p}n}$ and $a_{{\rm p}t}$ are given, then the system of equations becomes closed and can be solved for the parameters of i-th and j-th particles after their collision. In this case we can also calculate the Jacobian $J_1 = |D(\mathbf{y}^+_i, \mathbf{y}^+_j)/D(\mathbf{y}^-_i, \mathbf{y}^-_j)| = -a_{{\rm p}n}a^2_{{\rm p}t}$ and then the parameter J in the collisional integral: $J = a^2_{{\rm p}n}a^2_{{\rm p}t}$. In reality, the absolute values of $a_{{\rm p}n}$ and $a_{{\rm p}t}$ are always less than a unity, hence $J < 1$. The multiplier $1/J$ in the collisional integral takes into account the "compression" of the phase space caused by the losses of the kinetic energy of colliding particles.

In the present study the force $\mathbf{f}_{\rm p}$ acting on a particle includes the drag force $\mathbf{f}_{\rm D}$ and the lift Magnus force $\mathbf{f}_{\rm M}$ ($\mathbf{f}_{\rm p} = \mathbf{f}_{\rm D} + \mathbf{f}_{\rm M}$) which dominate over all other force components in the flow under consideration. These forces and the torque $\mathbf{l}_{\rm p}$ can be expressed in terms of the dimensionless coefficients $C_{\rm D}$, C_ω, and C_l:

$$\mathbf{f}_{\rm D} = \frac{1}{2}C_{\rm D}\pi r^2_{\rm p}\rho|\mathbf{v} - \mathbf{v}_{\rm p}|(\mathbf{v} - \mathbf{v}_{\rm p}), \qquad \mathbf{f}_{\rm M} = \frac{4}{3}C_\omega\pi r^3_{\rm p}\rho[(\mathbf{\Omega} - \mathbf{\Omega}_{\rm p}) \times (\mathbf{v} - \mathbf{v}_{\rm p})], \qquad \mathbf{l}_{\rm p} = \frac{1}{2}C_l r^5_{\rm p}\rho|\mathbf{\Omega} - \mathbf{\Omega}_{\rm p}|(\mathbf{\Omega} - \mathbf{\Omega}_{\rm p}), \tag{23}$$

where $\mathbf{\Omega} = (1/2)\mathrm{curl}\,\mathbf{v}$. The coefficients were calculated from the formulae approximating the analytical, experimental and numerical data in wide ranges of the governing parameters of the flow around a single particle.

The drag coefficient $C_{\rm D}$ was calculated from the approximation formula proposed in [21]:

$$C_{\rm D}({\rm Re}_{\rm p},\, {\rm M}_{\rm p},\, T_{\rm p}/T) = \begin{cases} C^1_{\rm D}, & 0 < \ {\rm M}_{\rm p} \le 1, \\ C^1_{\rm D1} + \dfrac{4}{3}({\rm M}_{\rm p} - 1)(C^2_{\rm D2} - C^1_{\rm D1}), & 1 < \ {\rm M}_{\rm p} \le 1.75, \\ C^2_{\rm D}, & {\rm M}_{\rm p} > 1.75, \end{cases}$$

where

$$C^1_{\rm D}({\rm Re}_{\rm p}, {\rm M}_{\rm p}, T_{\rm p}/T) = 24\left\{{\rm Re}_{\rm p} + \sqrt{\frac{\gamma}{2}}{\rm M}_{\rm p}\left[4.33 + \frac{3.65 - 1.53T_{\rm p}/T}{1 + 0.353T_{\rm p}/T}\exp\left(-0.247\sqrt{\frac{2}{\gamma}}\frac{{\rm Re}_{\rm p}}{{\rm M}_{\rm p}}\right)\right]\right\}^{-1}$$

$$+\left[\frac{4.5 + 0.38(0.03{\rm Re}_{\rm p} + 0.48\sqrt{{\rm Re}_{\rm p}})}{1 + 0.03{\rm Re}_{\rm p} + 0.48\sqrt{{\rm Re}_{\rm p}}} + 0.1{\rm M}^2_{\rm p} + 0.2{\rm M}^8_{\rm p}\right]\exp\left(-\frac{{\rm M}_{\rm p}}{2\sqrt{{\rm Re}_{\rm p}}}\right) + 0.6\sqrt{\frac{\gamma}{2}}{\rm M}_{\rm p}\left[1 - \exp\left(-\frac{{\rm M}_{\rm p}}{{\rm Re}_{\rm p}}\right)\right],$$

$$C^2_{\rm D}({\rm Re}_{\rm p}, {\rm M}_{\rm p}, T_{\rm p}/T) = \left[0.9 + \frac{0.34}{{\rm M}^2_{\rm p}} + 1.86\sqrt{\frac{{\rm M}_{\rm p}}{{\rm Re}_{\rm p}}}\left(2 + \frac{8}{\gamma{\rm M}^2_{\rm p}} + \frac{2.116}{\gamma{\rm M}_{\rm p}}\sqrt{\frac{T_{\rm p}}{T}} - \frac{4}{\gamma^2{\rm M}^4_{\rm p}}\right)\right]\cdot\left(1 + 1.86\sqrt{\frac{{\rm M}_{\rm p}}{{\rm Re}_{\rm p}}}\right)^{-1}.$$

Here ${\rm Re}_{\rm p} = 2\rho|\mathbf{v} - \mathbf{v}_{\rm p}|r_{\rm p}/\mu$ and ${\rm M}_{\rm p} = |\mathbf{v} - \mathbf{v}_{\rm p}|/\sqrt{\gamma\Re T}$ are the relative particle Reynolds and Mach numbers, $C^1_{\rm D1}$ is the value of $C^1_{\rm D}$ at ${\rm M}_{\rm p} = 1$, and $C^2_{\rm D2}$ is the value of $C^2_{\rm D}$ at ${\rm M}_{\rm p} = 1.75$. The dependence of $C_{\rm D}$ on $T_{\rm p}/T$ is very week in the flow under consideration. That is why we have ignored this dependence, and the ratio $T_{\rm p}/T = 1$ has been taken as unity.

For calculation of C_ω, the exact solution from [22] and the formula proposed in [23] were used

$$C_\omega = \begin{cases} 3/4, & 2\gamma_\omega < 0.45, \\ 3/8\ \hat{C}_\omega, & 2\gamma_\omega \ge 0.45, \end{cases} \tag{24}$$

DOI: 10.13009/EUCASS2019-455

where $\gamma_\omega = |\mathbf{\Omega} - \mathbf{\Omega}_\mathrm{p}| r_\mathrm{p}/|\mathbf{v} - \mathbf{v}_\mathrm{p}|$, $\hat{C}_\omega(\gamma_\omega, \mathrm{Re}_\mathrm{p}) = \gamma_\omega^{-1}[0.45 + (2\gamma_\omega - 0.45)\exp(-0.075\gamma_\omega^{0.4}\mathrm{Re}_\mathrm{p}^{0.7})]$.

The expression for the coefficient C_l was taken in the form proposed in [24]

$$C_l = \frac{C_{l1}}{\sqrt{\mathrm{Re}_{\mathrm{p}\omega}}} + \frac{C_{l2}}{\mathrm{Re}_{\mathrm{p}\omega}}, \tag{25}$$

where $\mathrm{Re}_{\mathrm{p}\omega} = \rho|\mathbf{\Omega} - \mathbf{\Omega}_\mathrm{p}| r_\mathrm{p}^2/\mu$, and constants C_{l1} and C_{l2} are given in the Table 2.

Table 2: Coefficients C_{l1} and C_{l2} in different ranges of the particle rotational Reynolds number $\mathrm{Re}_{\mathrm{p}\omega}$

$\mathrm{Re}_{\mathrm{p}\omega}$	C_{l1}	C_{l2}
$0 - 6$	0	16π
$6 - 20$	5.32	37.2
$20 - 50$	6.44	32.2
$50 - 4 \cdot 10^4$	6.45	32.1

5. Model of the carrier gas flow

In the present study we consider gas-particle flow over a cylinder. The particle volume fraction is assumed to be low enough so that the reversed effect of the particle phase on the carrier gas is negligible. This allows us to consider gas flow as two-dimensional (2D). We also consider not too high Reynolds number of flow over a cylinder so that the flow near a cylinder is laminar and can be described by the Navier–Stokes equations, which for the time-depended compressible 2D flow can be written in Cartesian coordinates (x, y) in the following compact form [25]:

$$\frac{\partial \mathbf{Q}}{\partial t} + \frac{\partial \mathbf{F}_x}{\partial x} + \frac{\partial \mathbf{F}_y}{\partial y} = \frac{\partial \mathbf{G}_x}{\partial x} + \frac{\partial \mathbf{G}_y}{\partial y}, \tag{26}$$

where the vectors $\mathbf{Q}$, $\mathbf{F}_x$, $\mathbf{F}_y$, $\mathbf{G}_x$ and $\mathbf{G}_y$ are defined as follows

$$\mathbf{Q} = \begin{pmatrix} \rho \\ \rho u \\ \rho v \\ \rho e \end{pmatrix}, \quad \mathbf{F}_x = \begin{pmatrix} \rho u \\ \rho u^2 + p \\ \rho uv \\ (\rho e + p)u \end{pmatrix}, \quad \mathbf{F}_y = \begin{pmatrix} \rho v \\ \rho uv \\ \rho v^2 + p \\ (\rho e + p)v \end{pmatrix}, \quad \mathbf{G}_x = \begin{pmatrix} 0 \\ \tau_{xx} \\ \tau_{xy} \\ u\tau_{xx} + v\tau_{xy} - q_x \end{pmatrix}, \quad \mathbf{G}_y = \begin{pmatrix} 0 \\ \tau_{xy} \\ \tau_{yy} \\ u\tau_{xy} + v\tau_{yy} - q_y \end{pmatrix}. \tag{27}$$

Here,

$$\tau_{xx} = \frac{2}{3}\mu\left(2\frac{\partial u}{\partial x} - \frac{\partial v}{\partial y}\right), \quad \tau_{yy} = \frac{2}{3}\mu\left(2\frac{\partial v}{\partial y} - \frac{\partial u}{\partial x}\right), \quad \tau_{xy} = \mu\left(\frac{\partial u}{\partial y} + \frac{\partial v}{\partial x}\right), \tag{28}$$

$$q_x = -\lambda\frac{\partial T}{\partial x}, \quad q_y = -\lambda\frac{\partial T}{\partial y}, \quad p = \rho RT, \quad e = c_v T + \frac{u^2 + v^2}{2}. \tag{29}$$

In these equations, t is the time; (xy) is the plane of flow, u and v are the x- and y-components of the velocity vector; ρ, p, e, T, μ and λ are the gas density, pressure, specific total energy, temperature, viscosity, and thermal conductivity, respectively; R is the gas constant; and c_V is the specific heat at constant volume. For μ and λ the following relations were used $\mu = \mu_s(T/T_s)^{3/2}(T_s + C_s)/(T + C_s)$ and $\lambda = c_p\mu/\mathrm{Pr}$, where the first relation is the Sutherlend formula (for the air $\mu_s = 1.71 \cdot 10^{-5}$ N·s/m^2, $T_s = 288$ K, $C_s = 117$ K); Pr is the Prandtl number; and c_p is the specific heat at constant pressure. The above system of equations is closed.

6. Gas-particle flow over a cylinder: results and discussion

At first, the equations (26)–(29) were solved numerically by CFD method with high accuracy. Steady-state flow was obtained as a limit of unsteady solution at large time (see Fig. 6). Total number of grid cells in the shock layer was about 250 thousands. A number of cells along the cylinder contour from the stagnation point to the maximal cross-section was one thousand, and across the boundary layer about 15. Input data for computational simulation were taken as follows: the cylinder diameter $D = 20$ mm, the free stream velocity $V_\infty = 600$ m/s, the pressure $p_\infty = 853$ Pa,

DOI: 10.13009/EUCASS2019-455

the temperature $T_\infty = 88.7$ K. These values correspond to the Mach number $M_\infty = 3.18$ and the Reynolds number $Re = \rho_\infty V_\infty D/\mu_\infty = 0.7 \cdot 10^5$. The Prandtl number was equal to $Pr = 0.71$. At the cylinder surface the normal and tangential velocity components were zero, the temperature was $T_w = 300$ K.

Interaction of a particle cloud with the cylinder in a supersonic two-phase gas-particle flow was studied numerically to investigate the role of rebounded particle scattering, particle-particle collisions and particle size distribution in formation of the particle phase flow structure. The initial position of a cloud ($L = 100$ mm, $B = 20$ mm), configuration of the bow shock wave, and field of the Mach number in the shock layer are shown in Fig. 6. Particles in an undisturbed flow were assumed to have the velocity and the temperature equal to those of the carrier gas. The carrier gas flow was considered as two-dimensional, but the motion of every particle was simulated as three-dimensional. The particle material density was equal to $\rho_p^\circ = 2650$ kg/m^3. The size of spherical particles was equal to their diameter d_p. For non-spherical particles, the size was considered as the diameter of spherical particles of the same volume (mass). In calculations the particle size was varied from 1 μm to 10 μm. These particle parameters together with the parameters taken for the gas flow correspond to the Stokes number $Stk = \rho_p^\circ d_p^2 V_\infty/(18\mu_\infty D)$ from 0.77 (particles of medium inertia) to 77 (coarse particles of high inertia).

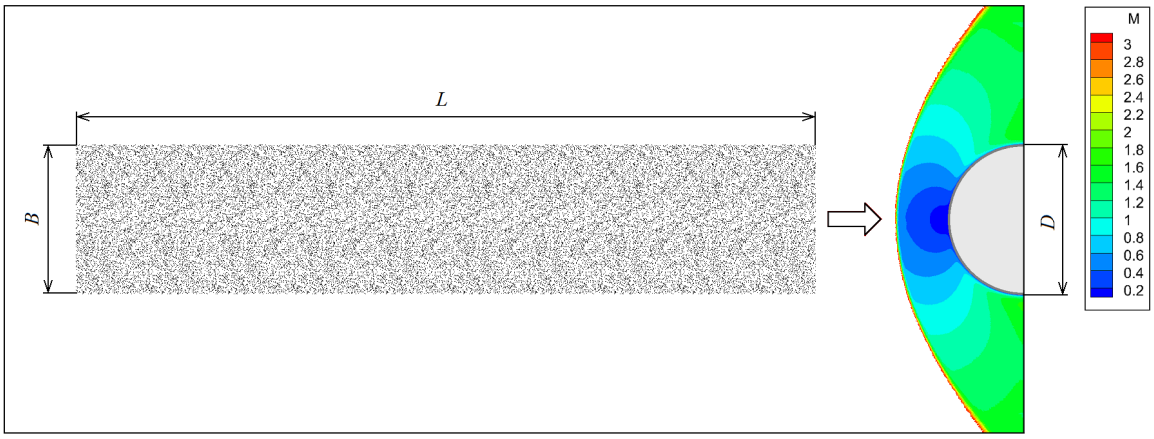

Figure 6: Particle cloud configuration in an undisturbed flow and field of Mach number in the shock layer.

The actual shape of non-spherical particles was taken into account only in simulation of particle rebounding from the cylinder surface. In all other "elementary" processes (particle-particle collisions and particle gas interaction) non-spherical particles were considered as spherical ones of the same volume.

Computational simulation of "collisional gas" of particles in the carrier gas flow was performed by the direct simulation Monte Carlo (DSMC) method described in detail in [26]. In calculations, the restitution coefficients entering the relation (22) were taken for colliding particles as follows: $a_{pn} = 0.5$ and $a_{pt} = 0.9$.

Instant patterns of distribution of spherical and prismatic particles near the forward part of a cylinder are shown in Fig. 7. As is seen, a particle shape influences the particle phase flow pattern very strongly. Prismatic particles fly off from the cylinder surface after rebound much farther than spherical ones of the same size. Coarse particles (10 μm) fly off even beyond the shock layer. At first glance such difference in behaviour of spherical and prismatic particles is unexpected, and an additional investigation was carried out to understand this phenomenon. For every non-spherical particle of fixed shape and every test angle of incidence, 50 million rebounds were calculated for different random particles' space orientation before an impact. The velocity impact of 500 m/s was close to those obtained in simulation of particle cloud interaction with a cylinder. The same collision model was used in all cases. The dimensionless particles' velocities and their normal and tangential components averaged over all tests *versus* the angle of incidence are presented in Fig. 8. The average velocity V_{p2} for all particles' shape turned out to be close to each other in the range $0 \leqslant \alpha_1 \lesssim 70^\circ$, however the difference increases with further increasing α_1 up to 90°. For spherical particles V_{p2} becomes very small at $\alpha_1 = 90^\circ$, whereas for prismatic particles and prismatic particles with cut vertices V_{p2} remains close to that at $\alpha_1 \approx 70^\circ$. A close examination of this result showed that a substantial normal and tangential velocities V_{n2} and $V_{\tau 2}$ appears for non-spherical particles even at normal impact ($\alpha_1 = 90^\circ$) due to multiple collisions (see Table 1) and twisting during rebound. Spherical particles experience only one collision at all values of α_1, and they are not twisted at $\alpha_1 = 90^\circ$.

The next part of the study deals with the effect of particle-particle collision. Figure 9 demonstrates this effect for different particle size, particle shape, and particle volume fraction $\alpha_{p\infty}$ in an initial cloud. We note that patterns of prismatic particles for $\alpha_{p\infty} = 10^{-4}$ are very close to those in Fig 7. This means that the effect of collisions at this particle concentration is negligible. An increase of $\alpha_{p\infty}$ up to 10^{-3} results in considerable change of the patterns for the

DOI: 10.13009/EUCASS2019-455

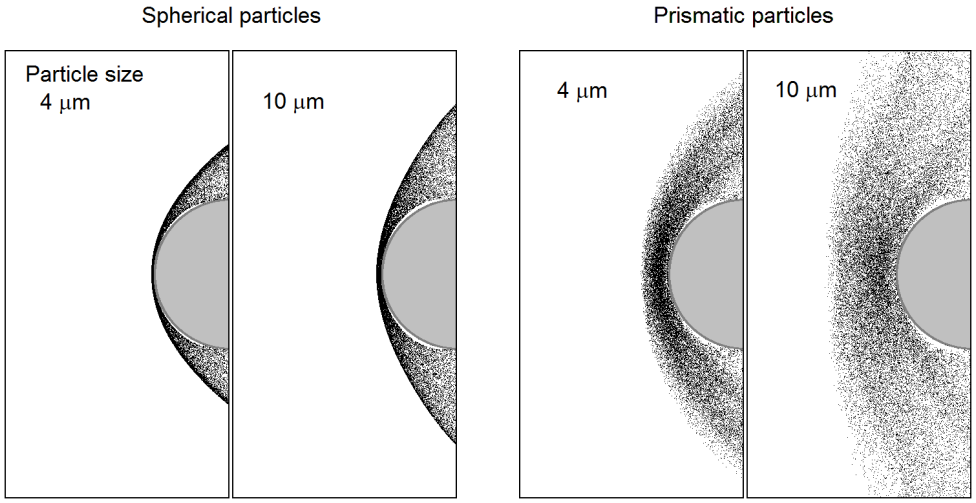

Figure 7: Instantaneous patterns of monosized particles near the forward part of a cylinder: particle-particle collisions are not taken into account.

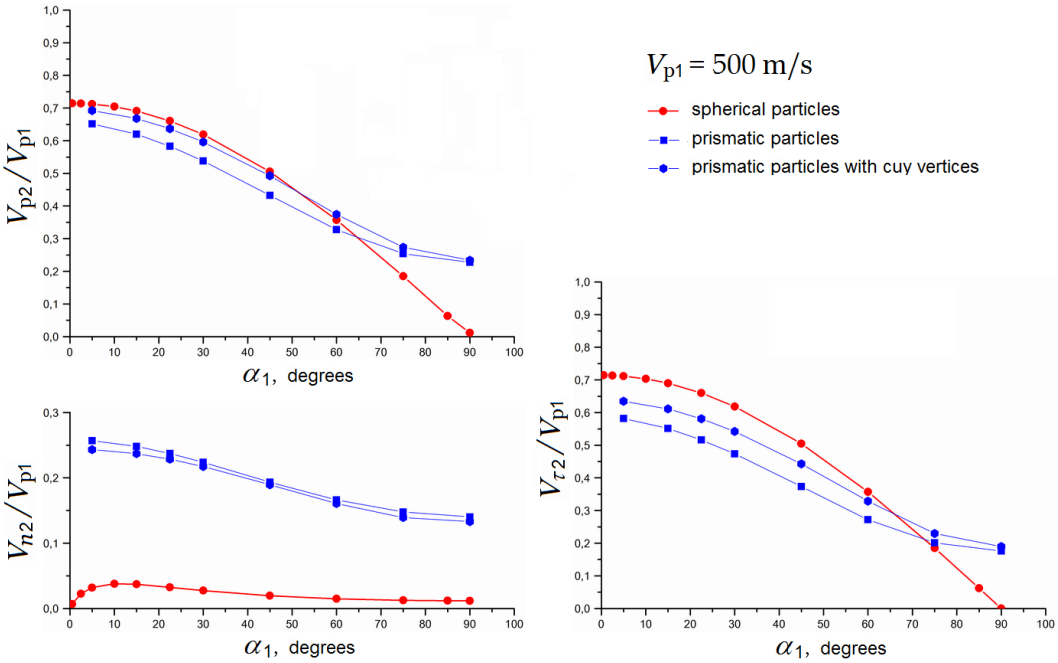

Figure 8: Mean restitution coefficients V_{p2}/V_{p1}, V_{n2}/V_{p1} and $V_{\tau 2}/V_{p1}$ as functions of the angle of incidence α_1 for different particle shape.

considered particle shapes and particle size. We note that for larger particle concentration ($\alpha_{p\infty} = 10^{-3}$) preliminary calculations were performed also for a two-way coupled gas-particle flow model. They shown a very weak effect in this case.

As is known, real particles never have the same size. The lognormal law for the particle distribution in size was taken in a initial particle cloud to study the effect of the particle size scatter on the particle phase flow pattern. This law has the form:

$$g_\infty(d_p) = \frac{1}{\sqrt{2\pi}\, d_p \log\sigma} \exp\left[-\left(\frac{\log d_p - \log d_g}{\sqrt{2}\log\sigma}\right)^2\right] \tag{30}$$

where parameter d_g is related with the most probable particle size d_{pm} by the formula $d_g = d_{pm}\exp(\log^2\sigma)$. Calculations were performed for $\sigma = 1.2$ and 1.728. Plots of g_∞ are shown in Fig. 10.

In Fig. 11 are given the particle phase flow patterns for $\sigma = 1.728$. It is seen that the effect of the particle size

DOI: 10.13009/EUCASS2019-455

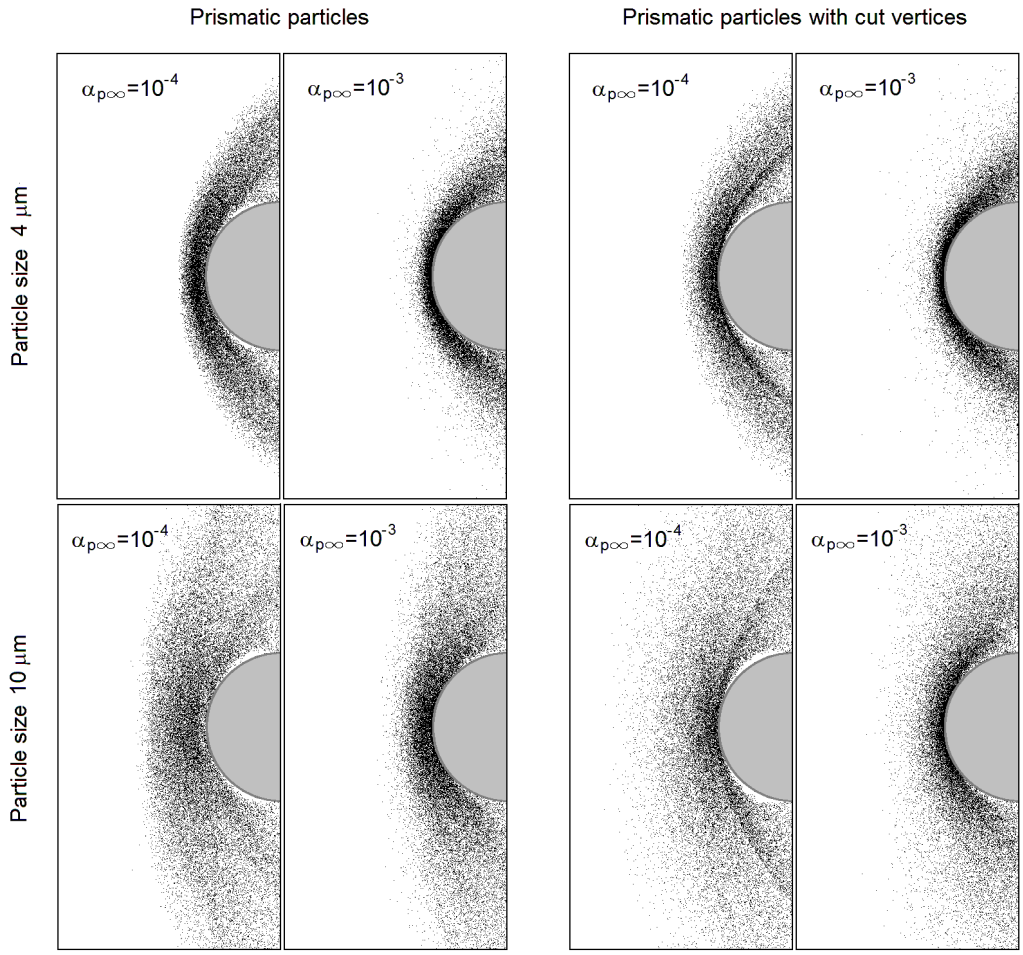

Figure 9: Effect of the particle-particle collisions on the particle phase flow pattern for different particle size, particle shape, and particle volume fraction $\alpha_{p\infty}$ in an undisturbed gas-particle flow.

scatter is noticeable. It should be noted that this effect for $\sigma = 1.2$ is practically invisible.

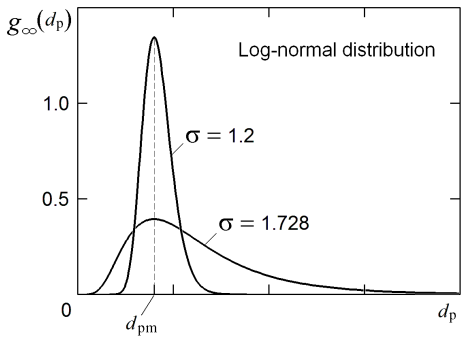

Figure 10: Lognormal law of particle size distribution in an initial cloud.

Besides investigation of the role of effect of random nature on particle phase flow patterns, the particle kinetic energy loss ΔE along the cylinder contour was calculated. Some results are displayed in Fig. 12 (E is the full particle kinetic energy flux in the undisturbed flow). This loss is caused by inelastic particle-wall collisions, and it depends on material properties of particles and a streamlined body (cylinder), particles' shape and size, flow velocity, particle-particle collisions, and some others. Based on the models taken in the present study, we can conclude that prismatic particles results in less decrease of energy loss than spherical particles almost on the whole forward part of a cylinder (in the range $0 \leqslant \theta \lesssim 70^\circ$). Particle-particle collisions additionally decrease energy loss that can be interpreted as the shielding effect.

DOI: 10.13009/EUCASS2019-455

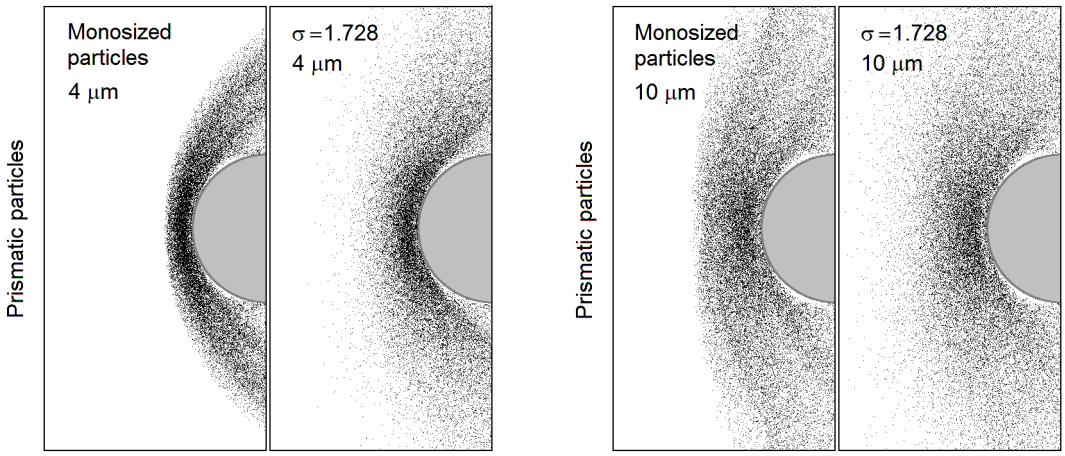

Figure 11: The effect of particle size distribution on the particle phase flow pattern.

The particle energy loss is distributed between rebounded particles, cylinder, and the carrier gas, however this distribution is unknown and requires further experimental and theoretical investigations. This question is of great importance for prediction of the body erosion rate in a gas-particle flow.

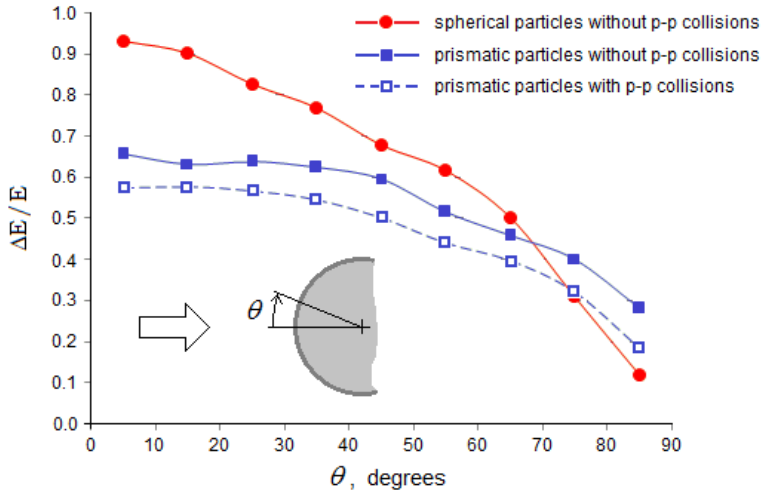

Figure 12: Effect of the particle shape and the particle-particle (p-p) collisions on the particle kinetic energy loss during particle phase interaction with the forward part of a cylinder. $\alpha_{p\infty} = 10^{-3}$.

7. Conclusion

Computational simulation of supersonic two-phase gas-particle flow over a blunt body (cylinder) was performed with taking account for the following effects of random nature: scattering of particles rebounded from the body surface due to non-spherical particle shape, collisions between particles, and particle size distribution. Two non-spherical particle shapes were considered: rectangular parallelepiped (prismatic particles) and rectangular parallelepiped with cut vertices, and the results were compared with those for spherical particles. Calculations were performed for medium to highly inertial particles (Stokes number was varied from a value of order of a unity to several tens). The most important conclusions are sum up below.

Rebounding of non-spherical particles is accompanied very often by two and more collisions. For example, 97 % prismatic particles in the case on normal impact experience more than one collision (Table 1). Such particles are strongly twisted, and the magnitude of their normal velocity after a rebound is much higher than that for spherical particles (Fig. 8). Non-spherical particles fly away from the forward part of a blunt body much farther than spherical ones of the same mass.

All considered random phenomena (scattering of rebounded particles, particle-particle collisions and particle

DOI: 10.13009/EUCASS2019-455

size distribution) have an effect on the particle phase flow pattern. The effect of scattering is of primary importance for any particle concentration. Collisions between particles begin to play a noticeable role for rather high particle concentration, when the particle mass load in the flow is close or greater than that for the carrier gas. Particle size distribution has a pronounced effect only if the size dispersion is high enough (e.g., at $\sigma \gtrsim 1.7$ in the lognormal law (30), Fig. 10).

The particle shape has a essential effect on the particle kinetic energy loss during rebounding. In the vicinity of the stagnation point, the loss of prismatic particles energy can be less by a factor ≈ 0.7 than that for spherical particles (Fig. 12). Collisions between particles result in formation of a dense layer of chaotically moving particles near the body surface. This layer inhibits the body surface from high-speed particles producing a shielding effect.

The present study has shown that all considered effects can play an important role in gas-particle flows over bodies, and they should be taken into account.

Acknowledgements

The present study was supported by the Russian Foundation for Basic Research.

References

[1] Mikhatulin, D.S., Polezhaev, Yu.V. and Reviznikov, D.L. 2007. *Heat Transfer and Destruction of Bodies in Supersonic Heterogeneous Flow*, Moscow, Yanus-K. [in Russian]

[2] Tsirkunov, Yu.M. 2001. Gas–particle flows around bodies – key problems, modeling and numerical analysis. *4th Int. Conf. on Multiphase Flow : CD-ROM Proceedings ICMF'2001*, Ed.: E. Michaelides. Paper No. 607, 31 p.

[3] Vasilevskii, E.B., Osiptsov, A.N., Chirikhin, A.V. and Yakovleva, L.V. 2011. Heat exchange on the front surface of a blunt body in a high-speed flow containing low-inertia particles. *Journal of Engineering Physics and Thermophysics*, Vol. 74, No. 6: 1399–1411.

[4] Golubkina, I.V., Osiptsov, A.N. and Sakharov, V.I. 2011. Supersonic low-concentration dusty-gas flow past a plane cylinder in the presence of an oblique shock wave interacting with the bow shock. *Fluid Dynamics,*, Vol. 46, No. 1: 51–63.

[5] Oesterle, B., Volkov, A.N. and Tsirkunov, Yu.M. 2013. Numerical investigation of two-phase flow structure and heat transfer in a supersonic dusty gas flow over a blunt body. *Progress in propulsion physics*. Vol. 5. TORUS PRESS /EDP Sciences: 441–456.

[6] Majid, A., Bauder, U., Herdrich, G. and Fertig, M. 2016. Two-Phase Flow Solver for Hypersonic Entry Flows in a Dusty Martian Atmosphere. *Journal of Thermophysics and Heat Transfer*, Vol. 30, No. 2: 418–428.

[7] Reviznikov, D.L., Sposobin, A.V. and Ivanov, I.E. 2018. A change in the structure of a flow under the action of highly inertial particle when a hypersonic heterogeneous flow passes over a body. *High Temperature*, Vol. 56, No. 6: 884–889.

[8] Varaksin, A.Yu. 2018. Gas-solid flows past bodies. *High Temperature*, Vol. 56, No. 2: 275–295.

[9] Haider, A. and Levenspiel, O. 1989. Drag coefficient and terminal velocity of spherical and nonspherical particles. *Powder Technology*, Vol. 58, No. 1: 63–70.

[10] Hölzer, A. and Sommerfeld, M. 2008. New simple correlation formula for the drag coefficient of non-spherical particles. *Powder Technology*, Vol. 184: 361–365.

[11] Hölzer, A. and Sommerfeld, M. 2009. Lattice Boltzmann simulations to determine drag, lift and torque acting on non-spherical particles. *Computers & Fluids* , Vol. 38: 572–589.

[12] Amelyushkin, I.A. and Stasenko, A.L. 2018. Interaction of a gas flow carrying nonspherical microparticles with a cross cylinder. *Journal of Engineering Physics and Thermophysics*, Vol. 91 No. 2: 288–299.

[13] Sommerfeld, M. 2002. Kinetic simulation for analysing the wall collision process of nonspherical particles. *Proc. of ASME FEDSM'2002*, Paper No. 31239, 10 p.

[14] Panfilov, S.V. and Tsirkunov, Yu.M. 2008. Scattering of nonspherical particles rebounding from a smooth and a rough surface in a high-speed gas-particle flow. *J. Appl. Mech. Tech. Phys.*, Vol. 49, No. 2: 222–230.

DOI: 10.13009/EUCASS2019-455

[15] Tsirkunov, Yu.M., Romanyuk, D.A. and Panfilov, S.V. 2011. Effects of particle mixing and scattering in the dusty gas flow through moving and stationary cascades of airfoils. *Progress in Propulsion Physics*, Vol. 2. EDP Sciences: 459–474.

[16] Arboleda, B.Q., Qadir, Z., Sommerfeld, M. and Beatove, S.L. 2014. Modelling the wall collision of regular non-spherical particles and experimental validation. *ASME FEDSM'2014 Proceedings*, Paper No. 21610, 12 p.

[17] Reviznikov, D.L., Sposobin, A.V. and Sukharev, T.Yu. 2017. Numerical simulation of the flow around a blunt body in supersonic polydisperse stream. *High Temperature*, Vol. 55, No. 3: 400–406.

[18] Crowe, C.T., Sommerfeld, M. and Tsuji, Y. 1998. *Multiphase Flows with Droplets and Particles*, CRC Press, Boca Raton.

[19] Lashkov, V. A. 1991. Experimental determination of the coefficients of restitution of particles in the flow of a gas suspension in a collision against the surface. *J. Eng. Phys. Thermophys*, Vol. 60, No. 2: 154–159.

[20] Volkov, A.N. and Tsirkunov, Yu.M. 2000. Kinetic model of a collisional admixture in dusty gas and its application to calculating flow past bodies. *Izv. Russian Akad. Nauk, Mekh. Zhidk. Gasa.* No. 3: 81–97. (Engl. tranl. *Fluid Dynamics.* Vol. 35, No. 3: 380–392.)

[21] Henderson, Ch.B. 1976. Drag coeccients of spheres in continuum and rarefied flows. *AIAA Journal*, Vol. 14, No. 6: 707–708.

[22] Rubinow, S.I. and Keller, J.B. 1961. The transverse force on a spinning sphere moving in a viscous fluid. *J. Fluid Mech.*, Vol. 11: 447–459.

[23] Oesterlé, B. and Bui Dinh, T. 1998. Experiments on the lift of a spinning sphere in a range of intermediate Reynolds numbers. *Experim. in Fluids*, Vol. 25: 16–22.

[24] Dennis, S.C.R., Singh, S.N. and Ingham, D.B. 1980. The steady flow due to a rotating sphere at low and moderate Reynolds numbers. *J. Fluid Mech.*, Vol. 101: 257–279.

[25] Anderson, D.A., Tannehill, J.C. and Pletcher, R.H. 1984. *Computational Fluid Mechnics and Heat Transfer*, Hemisphere Publ. Corp., New York.

[26] Volkov, A.N. and Tsirkunov, Yu.M. 2002. CFD/Monte Carlo simulation of collision-dominated gas-particle flows over bodies. *Proc. of ASME FEDSM'2002*, Paper No. 31222, 14 p.